Research Article | Vol. 25, No. 4 | 20 Feb 2017 | OPTICS EXPRESS A124

Optics EXPRESS

Polarization-selective ultra-broadband super absorber

YAN KAI ZHONG, SZE MING FU, WEIMING HUANG, DING RUNG, JIAN YI-WEN HUANG, PARAG PARASHAR, AND ALBERT LIN*

Department of Electronic Engineering, National Chiao-Tung Univeristy, Hsinchu, 30010, Taiwan
**hdtd5746@gmail.com*

Abstract: While a broadband metamaterial perfect absorber (MPA) has been implemented and proposed intensively in recent years, an ultra-broadband perfect absorber with polarization selectivity has not been realized in literature. In this work, we propose a configuration of polarization-selective (PS) MPA with ultra-wide absorption bandwidth. The aluminum wire grid is integrated on top of the ultrathin-metal-dielectric stacking. The transverse electric (TE) wave is blocked due to the requirement of zero tangential electric field at the metal surface. The transverse magnetic field can pass the aluminum wire-grids because the normal electric field can be supported by the surface charge density at the metal surface, and full absorption of the TM wave is accomplished by the metal-dielectric stacking beneath. Theoretical calculation using rigorously coupled wave analysis demonstrates the wavelength selectivity from λ = 1.98μm to λ = 11.74μm where the TE absorption is <0.04 while TM absorption is >0.95, using 300 nm thick aluminum (Al) wire grid with 16-pair SiO_2/Ti stacking. Additionally, the design is wavelength scalable by adjusting the dielectric thickness (t_{SiO2}) and the wire grid period (P) and height (t). The experimental result is demonstrated using Al grids and Ti/SiO_2, and the measured result fully supports the calculated prediction.

OCIS codes: (280.0280) Remote sensing and sensors; (310.6845) Thin film devices and applications; (230.4170) Multilayers; (160.3918) Metamaterials; (350.6050) Solar energy.

References and links

1. X. Zhang and Z. Liu, "Superlenses to overcome the diffraction limit," Nat. Mater. **7**(6), 435–441 (2008).
2. D. Schurig, J. J. Mock, B. J. Justice, S. A. Cummer, J. B. Pendry, A. F. Starr, and D. R. Smith, "Metamaterial electromagnetic cloak at microwave frequencies," Science **314**(5801), 977–980 (2006).
3. N. Liu, M. Mesch, T. Weiss, M. Hentschel, and H. Giessen, "Infrared perfect absorber and its application as plasmonic sensor," Nano Lett. **10**(7), 2342–2348 (2010).
4. H.-T. Chen, W. J. Padilla, M. J. Cich, A. K. Azad, R. D. Averitt, and A. J. Taylor, "A metamaterial solid-state terahertz phase modulator," Nat. Photonics **3**(3), 148–151 (2009).
5. D. Dregely, R. Taubert, J. Dorfmüller, R. Vogelgesang, K. Kern, and H. Giessen, "3D optical Yagi-Uda nanoantenna array," Nat. Commun. **2**, 267 (2011).
6. X. Liu, T. Tyler, T. Starr, A. F. Starr, N. M. Jokerst, and W. J. Padilla, "Taming the blackbody with infrared metamaterials as selective thermal emitters," Phys. Rev. Lett. **107**(4), 045901 (2011).
7. C. Wu, B. Neuner III, J. John, A. Milder, B. Zollars, S. Savoy, and G. Shvets, "Metamaterial-based integrated plasmonic absorber/emitter for solar thermo-photovoltaic systems," J. Opt. **14**(2), 024005 (2012).
8. A. Polman and H. A. Atwater, "Photonic design principles for ultrahigh-efficiency photovoltaics," Nat. Mater. **11**(3), 174–177 (2012).
9. Q. Gan, F. J. Bartoli, and Z. H. Kafafi, "Plasmonic-enhanced organic photovoltaics: breaking the 10% efficiency barrier," Adv. Mater. **25**(17), 2385–2396 (2013).
10. C. M. Watts, X. Liu, and W. J. Padilla, "Metamaterial electromagnetic wave absorbers," Adv. Mater. **24**(23), 98–120 (2012).
11. W. H. Emerson, "Electromagnetic wave absorbers and anechoic chambers through the years," IEEE Trans. Antenn. Propag. **21**(4), 484–490 (1973).
12. B. A. Munk, *Frequency Selective Surfaces: Theory and Design* (John Wiley & Sons, 2000).
13. A. Kadambi, V. Taamazyan, B. Shi, and R. Raskar, "Polarized 3D: High-Quality Depth Sensing with Polarization Cues," in *IEEE International Conference on Computer Vision (ICCV)* (2015).
14. J. Chu, Z. Wang, Z. L. Le Guan, Y. Wang, and R. Zhang, "Integrated polarization dependent photodetector and its application for polarization navigation," IEEE Photonics Technol. Lett. **26**(5), 469–472 (2014).

#275951 https://doi.org/10.1364/OE.25.00A124
Journal © 2017 Received 30 Sep 2016; revised 9 Jan 2017; accepted 14 Jan 2017; published 3 Feb 2017

Optics EXPRESS

15. H. Tao, C. M. Bingham, D. Pilon, K. Fan, A. C. Strikwerda, D. Shrekenhamer, W. J. Padilla, X. Zhang, and R. D. Averitt, "A dual band terahertz metamaterial absorber," J. Phys. D Appl. Phys. **43**(22), 225102 (2010).
16. Q.-Y. Wen, H.-W. Zhang, Y.-S. Xie, Q.-H. Yang, and Y.-L. Liu, "Dual band terahertz metamaterial absorber: Design, fabrication, and characterization," Appl. Phys. Lett. **95**(24), 241111 (2009).
17. M. G. Deceglie, V. E. Ferry, A. P. Alivisatos, and H. A. Atwater, "Design of nanostructured solar cells using coupled optical and electrical modeling," Nano Lett. **12**(6), 2894–2900 (2012).
18. T. Lanz, B. Ruhstaller, C. Battaglia, and C. Ballif, "Extended light scattering model incorporating coherence for thin-film silicon solar cells," J. Appl. Phys. **110**(3), 033111 (2011).
19. F. J. Beck, S. Mokkapati, and K. R. Catchpole, "Light trapping with plasmonic particles: beyond the dipole model," Opt. Express **19**(25), 25230–25241 (2011).
20. K. Söderström, F.-J. Haug, J. Escarré, O. Cubero, and C. Ballif, "Photocurrent increase in n-i-p thin film silicon solar cells by guided mode excitation via grating coupler," Appl. Phys. Lett. **96**(21), 213508 (2010).
21. C. Min, J. Li, G. Veronis, J.-Y. Lee, S. Fan, and P. Peumans, "Enhancement of optical absorption in thin-film organic solar cells through the excitation of plasmonic modes in metallic gratings," Appl. Phys. Lett. **96**(13), 133302 (2010).
22. P. N. Saeta, V. E. Ferry, D. Pacifici, J. N. Munday, and H. A. Atwater, "How much can guided modes enhance absorption in thin solar cells?" Opt. Express **17**(23), 20975–20990 (2009).
23. K. Aydin, V. E. Ferry, R. M. Briggs, and H. A. Atwater, "Broadband polarization-independent resonant light absorption using ultrathin plasmonic super absorbers," Nat. Commun. **2**, 517 (2011).
24. O. Deparis and O. El Daif, "Optimization of slow light one-dimensional Bragg structures for photocurrent enhancement in solar cells," Opt. Lett. **37**(20), 4230–4232 (2012).
25. S. Hänni, G. Bugnon, G. Parascandolo, M. Boccard, J. Escarré, M. Despeisse, F. Meillaud, and C. Ballif, "High-efficiency microcrystalline silicon single-junction solar cells," Prog. Photovolt. Res. Appl. **21**, 821–826 (2013).
26. C. Battaglia, C.-M. Hsu, K. Söderström, J. Escarré, F. J. Haug, M. Charrière, M. Boccard, M. Despeisse, D. T. Alexander, M. Cantoni, Y. Cui, and C. Ballif, "Light trapping in solar cells: can periodic beat random?" ACS Nano **6**(3), 2790–2797 (2012).
27. A. Naqavi, K. Söderström, F.-J. Haug, V. Paeder, T. Scharf, H. P. Herzig, and C. Ballif, "Understanding of photocurrent enhancement in real thin film solar cells: towards optimal one-dimensional gratings," Opt. Express **19**(1), 128–140 (2011).
28. B. Zhang, Y. Zhao, Q. Hao, B. Kiraly, I.-C. Khoo, S. Chen, and T. J. Huang, "Polarization-independent dual-band infrared perfect absorber based on a metal-dielectric-metal elliptical nanodisk array," Opt. Express **19**(16), 15221–15228 (2011).
29. F. Hu, T. Zou, B. Quan, X. Xu, S. Bo, T. Chen, L. Wang, C. Gu, and J. Li, "Polarization-dependent terahertz metamaterial absorber with high absorption in two orthogonal directions," Opt. Commun. **332**, 321–326 (2014).
30. X. Xiong, Z.-H. Xue, C. Meng, S.-C. Jiang, Y.-H. Hu, R.-W. Peng, and M. Wang, "Polarization-dependent perfect absorbers/reflectors based on a three-dimensional metamaterial," Phys. Rev. B **88**(11), 115105 (2013).
31. Y.-L. Liao and Y. Zhao, "A wide-angle broadband polarization-dependent absorber with stacked metal-dielectric grating," Opt. Commun. **370**, 245–249 (2016).
32. J. Zhou, A. F. Kaplan, L. Chen, and L. J. Guo, "Experiment and theory of the broadband absorption by a tapered hyperbolic metamaterial array," ACS Photonics **1**(7), 618–624 (2014).
33. D. Ji, H. Song, X. Zeng, H. Hu, K. Liu, N. Zhang, and Q. Gan, "Broadband absorption engineering of hyperbolic metafilm patterns," Sci. Rep. **4**, 4498 (2014).
34. C. Argyropoulos, K. Q. Le, N. Mattiucci, G. D'Aguanno, and A. Alu, "Broadband absorbers and selective emitters based on plasmonic Brewster metasurfaces," Phys. Rev. B **87**(20), 205112 (2013).
35. Y. Cui, K. H. Fung, J. Xu, H. Ma, Y. Jin, S. He, and N. X. Fang, "Ultrabroadband light absorption by a sawtooth anisotropic metamaterial slab," Nano Lett. **12**(3), 1443–1447 (2012).
36. Y. K. Zhong, S. M. Fu, N. P. Ju, M. Tu, B. Chen, and A. Lin, "Fully planarized perfect metamaterial absorbers with no photonic nanostructures," IEEE Photonics J. **8**(1), 2200109 (2016).
37. M. G. Moharam and T. K. Gaylord, "Rigorous coupled-wave analysis of metallic surface-relief gratings," J. Opt. Soc. Am. A **3**(11), 1780–1787 (1986).
38. Rsoft, *Rsoft CAD User Manual,* 8.2 ed. (Rsoft Design Group, 2010).
39. Y. K. Zhong, "The broadband and selective perfect absorbers for thermophotovoltaics and sensing," Ph.D. Thesis (National Chiao-Tung University, Taiwan, 2017).
40. Y. K. Zhong, Y.-C. Lai, M.-H. Tu, B.-R. Chen, S. M. Fu, P. Yu, and A. Lin, "Omnidirectional, polarization-independent, ultra-broadband metamaterial perfect absorber using field-penetration and reflected-wave-cancellation," Opt. Express **24**(10), A832–A845 (2016).
41. X. J. Yu and H. S. Kwok, "Optical wire-grid polarizers at oblique angles of incidence," J. Appl. Phys. **93**(8), 4407–4412 (2003).

1. Introduction

Metamaterial perfect absorbers (MPA) have been a field of intensive research for many years due to its numerous applications in diverse fields [1–9]. These include superlenses [1], highly sensitive sensors [3], ultrafast modulators [4], antenna systems [5], thermal emitters [6], thermophotovoltaics [7], biomedical optics [10,11], and radar cross section (RCS) reduction

Optics EXPRESS

[12]. In many applications, the polarization dependent absorption is desired. The polarization information of the received optical signals can further increase the depth accuracy of detected images [13,14], and therefore, is of high interest to remote and geographical sensing, biomedical imaging, cyber-physical interfacing, internet of things, robotics, radar, and CMOS image sensors. Both narrow-band and broadband metamaterial perfect absorbers have been proposed and implemented. The ease of confining photons at a specific wavelength via various optical phenomena facilitates the implementation of narrowband MPAs, such as guided mode resonances [15–22], plasmonic resonances [21,23], slow-light absorption enhancement [24], and photonic density of states (PDOS) engineering in periodic structures [18,25–27]. Thus, it is relatively easier to construct a perfect absorption at narrow spectral range. The polarization-dependent narrowband MPAs have also been demonstrated in the literature [23,28–30]. Based our literature review, there has not been many efforts in realizing polarization-dependent ultra-broadband MPAs to date except the recent theoretical work by Liao et. al [31] in 2016. In [31], simulation result suggests the realization of a broadband polarization-dependent MPA by using varied-thickness layered metal-dielectric grating. The slight drawback is the absorption ripples exist in the high absorption band. In our proposal, we provide a different configuration with experimental verification. It will be shown that a wider bandwidth and higher absorption can be achieved using the proposal in this work. In addition, the fabrication complexity is reduced since only aluminum grid etching is necessary.

In contrast to narrowband perfect absorption, ultra-broadband absorption can be quite challenging since it is difficult to find an optical absorption phenomenon that can exist consistently over a broad spectral range. In literature, several decent efforts have been proposed recently to implement the broadband MPA without polarization-selection [32–35]. The past efforts on purely broadband metamaterial perfect absorbers without polarization-selection have been developed using patterned metallic grating on dielectric [15,16], metallic nanocones [34], and hyperbolic metamaterial (HMM) tapers [33,35]. An unprecedented adiabatically-coupled ultra-long tapered hyperbolic metamaterial (HMM) with a extremely wide absorption band were introduced by Fang et al. [35]. In this configuration, layer-by-layer metal-dielectric tapered structure is used in order to achieve a broad absorption band. In this scenario, the incident photons are coupled into the metallic films from the side of the HMM nano-tips or nanocones, and the photons of different wavelengths are absorbed by different portions of the HMM stacking. In our recent publications [36], we proposed a planar multiple thin-metal-dielectric stack configuration for MPAs that facilitates both simple fabrication and broadband omnidirectional absorption comparable to tapered HMM absorbers. The underlying physics of field penetration and field dissipation at the ultra-thin metallic films has been adopted here. As compared to tapered HMM perfect absorbers structure, this design eradicates the need for lithography and etching processes and, therefore, is totally scalable to large-area photonic applications. The additional advantage of fully planarized structure over MPAs using photonic nanostructures includes the easy integration with other optical components such as filters and polarizers. The metallic thin wire-grid polarizer is one of the most well-known sub-wavelength optical devices that split orthogonally polarized electromagnetic waves into a transmitted wave and a re□ected wave. High conductivity metals can serve the purpose of building wire-grid polarizers due to their large imaginary dielectric constants provides a nearly perfect electric conductor (PEC) boundary condition at metal-grid and air interface. These metallic grating could be used as polarizers [37], and could be implemented with other photonic structures such as planar MPAs.

In this paper, we report the integration of a thin metal based wire-grid polarizer on the planar MPA to harness the structural advantages of polarization selection with ultra-wide bandwidth offered by MPAs. Figure 1 is the schematic of the proposed design. A one-dimensional (1D) Al grid is laid over a planar MPA structure. Planer MPA structure consists of 15.5 pairs of repeated dielectric-metal stacks on a Ti substrate. P, W_{Al} and t are the period,

Optics EXPRESS

width and thickness of the metallic wire grid, respectively, to be imposed on the planar MPA structure. We believe the proposed polarization-dependent MPA is very useful for remote sensing, image reconstruction, biomedical imaging, detection, etc.

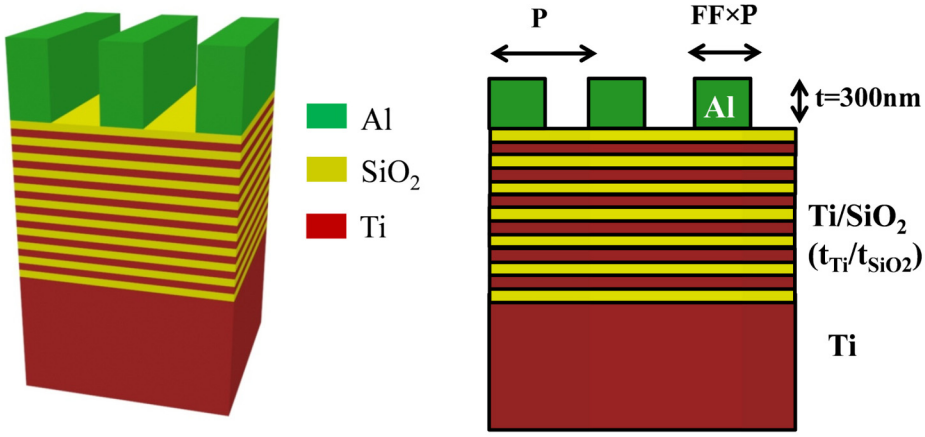

Fig. 1. The three-dimensional (3D) and two-dimensional (2D) cross-section plots of the proposed polarization-selective (PS) metamaterial absorber (MPA). Structure parameters are indicated.

2. Simulation

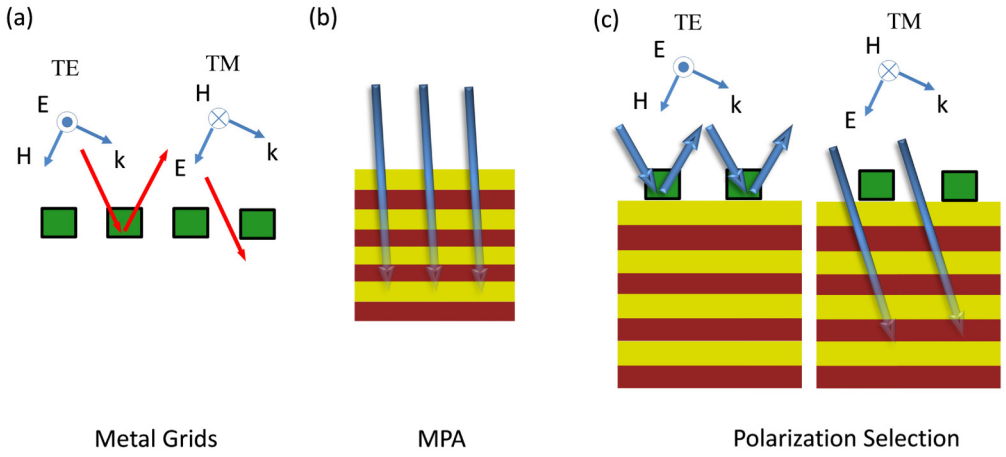

Fig. 2. The physics and design concept of the proposed polarization-selective (PS) MPA. Polarization selection is achieved by integrating metal grids with planar thin metal MPA. (a) The selection of the TE and TM wave by high extinction metal grids. (b) Broadband absorption by thin-metal-dielectric stacking. (c) The PS-MPA implementation. The key to the seamless integration lies in the planar nature of the MPA underneath and its broadband omnidirectional absorption. The near-field distribution after the wave passes the metal grids can have multiple diffraction orders, and thus omnidirectionality of the MPA is critical.

As illustrated in Fig. 1, the structure consists of repeated dielectric-metal stacks. The refractive indices (n) and extinction coefficients (k) from the Rsoft^{TM} material database [38] are used in this study. Since higher extinction metals like gold (Au), silver (Ag), or even aluminum (Al) leads to excessive reflection, moderate to lower extinction metals such as titanium (Ti), tungsten (W), and nickel (Ni) could be adopted for the periodic stacking of the ultra-thin metal and dielectric, in order to facilitate the field penetration effect in this planar MPA structure. On the other hand, for the wire-grid polarizer, high extinction metals such as

Au, Ag, Al are preferred. This is due to the high extinction metals can better approximate the perfect electric conductor with high surface charge density and close-to-zero skin depth. The minimal skin-depth is the key to the TE wave blocking in the wire grid polarizers, which are integrated into planar MPA design in this proposal to realize polarization-selectivity. For the selection of dielectric materials, lower index materials are preferred to reduce the air-dielectric reflection. Nevertheless, in order to reduce the total device thickness, higher index materials can also be used with the design of anti-reflection coating (ARC) [39]. Higher extinction metals, instead of Ti, can also be used to reduce the required pair number for perfect absorption, but this is at the cost of reduced bandwidth [36]. The Ni/SiO_2 data and the determination of the required pair number can be referred to in our past publication [40] where a single layer ultrathin metal absorption is shown, which can be used to estimate the required pair number for perfect absorption. The physics of the proposed polarization-selective (PS) MPA is illustrated in Fig. 2.

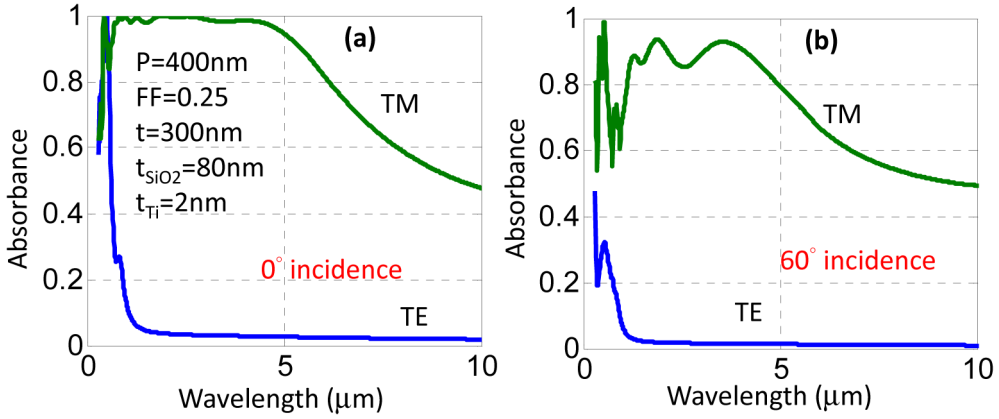

Fig. 3. The spectral response for the polarization-selective (PS) broadband MPA using Ti/SiO_2 stacking and a Al wire-grid. The period (P), fill factor (FF), aluminum grid thickness (t), oxide and titanium thicknesses (t_{SiO2}, t_{Ti}) are labeled in the figure inset. The spectral absorption at normal incidence and at oblique incidence (60°) are shown. 15.5-pair SiO_2/Ti is used.

It is worth reviewing the physics behind the highly-conductive metal wire grids. According to Maxwell's boundary conditions: In the absence of any static charge density at the interface between metal and dielectric, tangential electric field component is continuous at the interface, i.e, the tangential component of electrical field at the metal surface (E_{tm}) is equal to tangential component of electrical field at the air surface (E_{ta}).

$$E_{tm} = E_{ta} \tag{1}$$

Therefore, for TE polarization, the electric field is all at the tangential direction, and once the wave passes through the highly conductive metal grids, the electric field is forced to zero due to the requirement of zero electric field at the metal interior. On the other hand, the metal can support surface charge, and thus the normal component of the electric field does not have to vanish at air-metal boundary. The normal electric field satisfies

$$\varepsilon_0 E_{na} = \rho_{sm} \tag{2}$$

at air-metal interface. E_{na} is the normal component of the electric field in air, and ρ_{sm} is the metal surface charge density.

The simulation conducted here is based upon rigorous coupled wave analysis (RCWA). The RCWA is a numerical method that is classically applied in solving scattering from periodic structures in computational electromagnetism. Spectral absorbance is calculated in our analysis by RCWA with Diffractmod^{TM}. The eigenmodes of the layered periodic

Optics EXPRESS

waveguide structures are the expansion bases in the software, and therefore the bases are quite different from the traditional Fourier Modal Method (FMM). It is more natural to employ eigenmodes of the periodic structure itself to expand the solution fields, and this extensively improves convergence especially in the presence of metallic layers in the calculation domains.

Figure 3 shows the spectral absorption for the proposed wire-grid MPA. It is shown that strong polarization dependence is established by using a highly-conductive metal grid on top of the ultrathin metal-dielectric stacking. The spectral absorption of the TE wave is around 0.03, while the spectral absorption of the TM wave is around 0.98. Further decreased of the TE absorption can be done by replacing Al with Au or Ag, but Au and Ag are not compatible with silicon IC processing and thus preventing the photonics/electronics integration in silicon photonics platform. The physics associated with the polarization selectivity has been explained using the boundary conditions of Maxwell's equations in the previous paragraph, and the broadband absorption is based on the field penetration phenomenon in the ultrathin metallic films [36]. It is interesting to note that the selection of the ultrathin metal in metal-dielectric stacking should be moderate-extinction metals to realize field penetration while for the selection of the metal wire grid, high extinction metals should be used. The angular absorption is shown in Fig. 3(b). It can be seen that the polarization-selective absorption can persist until 60° incidence angle. This is because the underlying MPA possesses a wide receiving angle, and the wire-grid polarizer does not degrade significantly with incidence angles until 60°. The physics behind broadband wide-angle MPAs has been explained in [36], and the physics behind wide-angle wire-grid polarizers is explained in [41]. In current design, we use periodic stacking for Ti/SiO_2 MPA, and aperiodic design can further increase the polarization-selective absorption bandwidth.

The change of the polarization-selective absorption with varied geometry is shown in Fig. 4. In fact, the proposed design has large geometrical dimension tolerance where wideband polarization-selective absorption can exist for a broad range of geometrical parameters. Figure 4(a) shows the polarization-selective absorption dependence on the oxide spacer thickness (t_{SiO2}) in the MPA. The design guideline for thin-metal MPAs has been discussed in [36] regarding t_{SiO2} and t_{Ti}. The increase of t_{SiO2} leads to the absorption band being shifted to longer wavelength. On the other hand, the wire-grid polarizer possesses very broadband width, evident from RCWA [37] and from many commercially available modules. The bandwidth of the polarizer can be easily designed to >10μm due to the physics behind the polarization selection using wire-grids only weakly depends on wavelength. As a result, in Fig. 4(a) polarizer bandwidth is not a limiting factor, and as the MPA absorption bandwidth is shifted toward longer wavelength by increasing t_{SiO2}, the polarization-selective absorption band is shifted accordingly achieving wavelength scalability. It is also worth to mention that for the case of t_{SiO2} = 500nm in Fig. 4(a), an ultra-broadband polarization-selective absorption is demonstrated from λ = 1.98μm to λ = 11.74μm where the TE absorption is <0.04 while TM absorption is >0.95. In Fig. 4(b), the dependence of polarization-selective absorption on the aluminum grating fill factor (FF) is shown. For gradually increased FF, the TM absorption can decrease due to the slits between the Al grating becomes too narrow for transmission. On the other hand, TE blocked transmission/absorption is not affected by the increased FF. In Figs. 4(c) and 4(d), the dependencies of polarization-selective absorption on the Al wire-grid period (P) and thickness (t) are studied. It is observed that the proposed design is robust against geometrical parameters where the variation in P from 400nm to 1μm and the change in t from 100nm to 500nm do not significantly alter the TE and TM absorption.

Optics EXPRESS

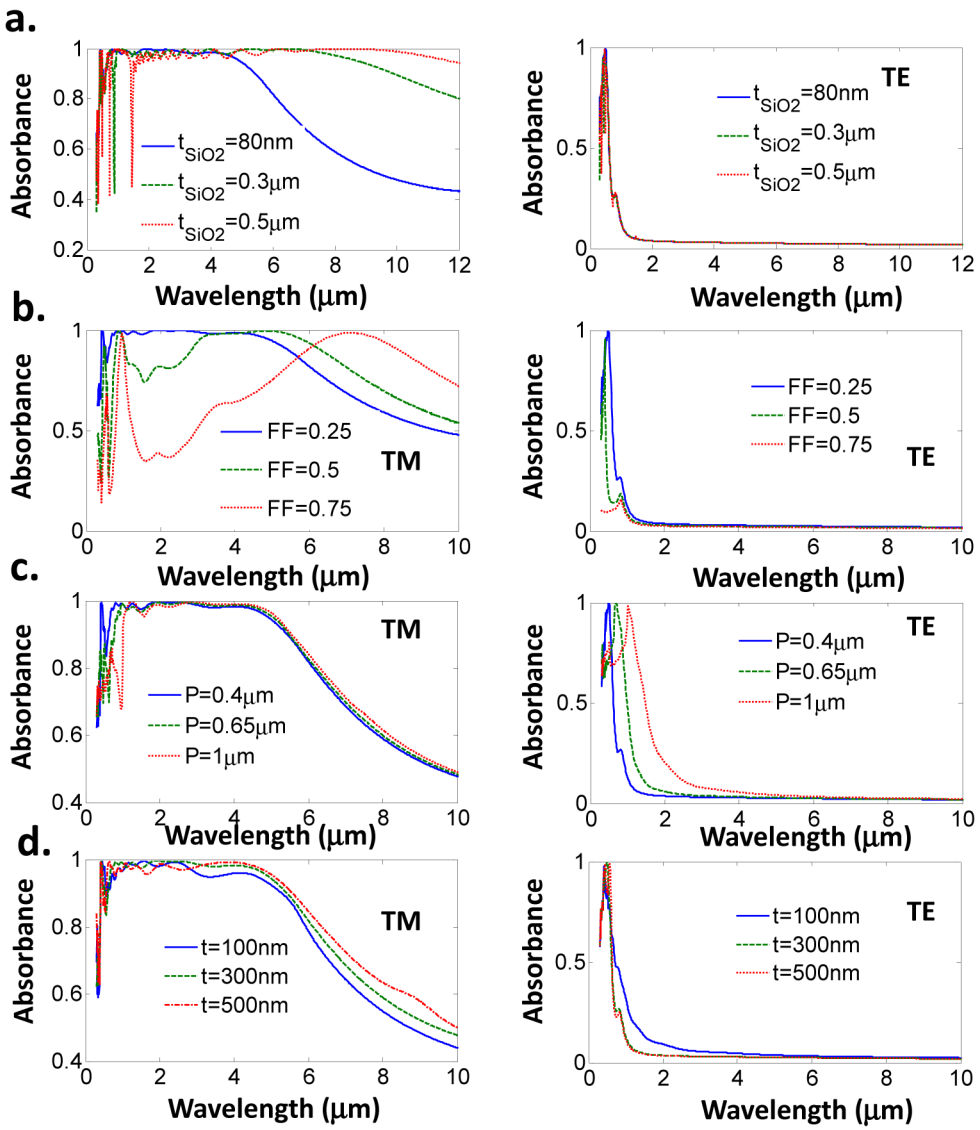

Fig. 4. The variation of the polarization-selective absorption with different geometrical parameters. The baseline parameters are t_{SiO2} = 80nm, t_{Ti} = 2nm, P = 400nm, FF = 0.25, t = 300nm. 15.5-pair SiO_2/Ti is used. The variation of the geometrical parameters is labeled in the legends. (a) Sweep on the dielectric spacer thickness in bottom MPA (t_{SiO2}). (c) Sweep on the aluminum wire grid fill factor (FF). (c) Sweep on the aluminum wire grid period (P). (d) Sweep on the aluminum wire grid thickness (t).

Figure 5 plots the field profiles for various field components at λ = 5μm for the geometry in Fig. 3(a). We can see that the penetration of the TM wave into the stacking of ultrathin Ti and dielectric. On the other hand, the TE wave is blocked by the Al metal grids and not able to reach the Ti/SiO_2 stacking. Slight encroachment of the field intensity into Al grids can be observed in Fig. 5(d), and this reflects the physical reason that 3% absorption can still be observed for the TE wave in Fig. 3. Perfect electric conductors can totally eliminate the residual absorption. Using Ag or Au can certainly be beneficial in this regard but leads to contamination in silicon IC processing.

Optics EXPRESS

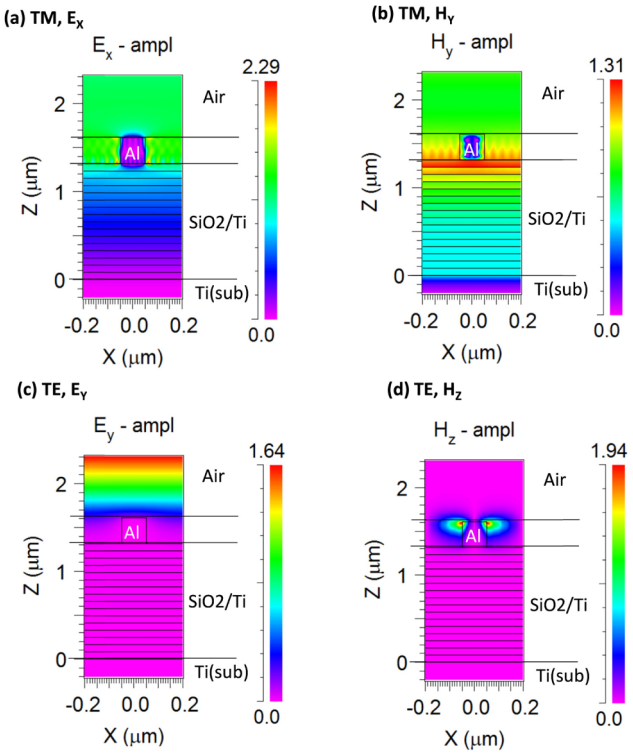

Fig. 5. The TE/TM field profiles for the polarization-selective broadband MPA at λ = 5μm. The field amplitude at harmonic steady state for various field components (E_x, E_y, H_y, H_z) are plotted. The geometry is the same as Fig. 3(a).

3. Experiment

A bare silicon wafer is used for the deposition of 500nm Ti bottom layer. After that, 15 alternating pairs of SiO_2/Ti layers are deposited on this Ti bottom layer, starting from SiO_2 deposition. One more layer of SiO_2 is also deposited at the top of this planar MPA structure, and thus totally 15.5 pairs of SiO_2/Ti is deposited. AST PEVA 600I electron gun (e-gun) evaporators are used for the deposition of the SiO_2/Ti based MPA structure. The deposition pressure of 3×10^{-6} and 5×10^{-6} torr without substrate heating is maintained for the deposition of Ti and SiO_2 films, respectively. The deposition rate for Ti and SiO_2 films via e-gun evaporation have been reported as 0.5nm/sec for Ti and 0.2nm/sec for SiO_2, respectively. Deposition pressure and rate play a vital role for the optimization of the surface roughness and thin film morphology. Furthermore, molecular beam epitaxy (MBE), atomic layer deposition (ALD), and metalorganic chemical vapor deposition (MOCVD) could be employed for a fully smooth film. A 500nm Ti layer is deposited on the wafer backside to eliminate any residual transmittance.

Optics EXPRESS

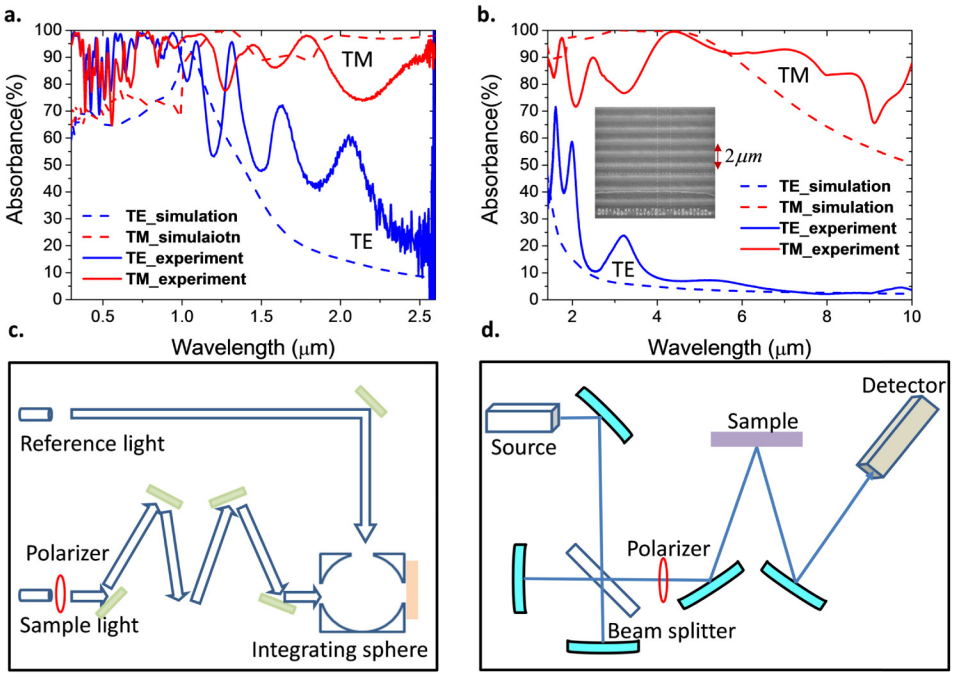

Fig. 6. (a) The normal incidence spectral absorption of the polarization-selective broadband MPA in the UV-VIS-NIR regime. (b) The normal incidence spectral absorption from λ = 1.24μm to λ = 10μm spectrum using FTIR. The geometry is P = 1μm, FF = 0.3, t_{Ti} = 2nm, t_{SiO2} = 80nm. The aluminum grid thickness (t) is 300nm. 15.5 pairs of Ti/SiO_2 are used. (c) The schematic diagram of UV-VIS-NIR and (d) the schematic diagram of FTIR measurement

For the metallic grid polarizer, a 300nm Al layer is deposited on this planar MPA structure via e-gun evaporation. Afterward, e-beam lithography with Leica™ Weprint 200 E-Beam stepper is used for exposure. Sumitomo™ NEB-22 negative-tone resist with resolution ~100nm is employed. The development of the exposed resist is by tetramethylammonium hydroxide (TMAH). After development, the etching of the Al grid is achieved by ICP etching using Lam Research ™ TCP 9600SE using mixture of Cl_2 and BCl_3. The resist removal is done by Fusion™ Ozone 200 AC/II Asher and then by the solution consisting of 8% H_2SO_4 and 4% H_2O_2 at 45°C for 120 seconds. Afterward, acetone, isopropyl alcohol (IPA), and deionized (DI) water clean is conducted to fully remove the resist. Measurement of the absorbance is done by measuring the reflectance (R) and the transmittance (T), and then the absorbance (A) is calculated by A = 1-R-T. The Hitachi U-4100 UV-VIS-NIR spectrometer and the Bruker™ IFS 66v/S Fourier transform infrared (FTIR) spectroscopy are used for this purpose.

The measurement results along with the corresponding calculated results are shown in Fig. 6. The Period P = 1μm, the aluminum grid thickness is t = 300nm, and the fill factor is FF = 0.3. 15.5 pairs of Ti/SiO_2 are deposited with t_{SiO2} = 80nm and t_{Ti} = 2nm. Further increase in t_{SiO2} can shift the MPA absorption bandwidth to longer wavelength regimes. The absorption bandwidth for the PS-MPA with t_{SiO2} = 80nm is from λ = 4μm to λ = 8μm. The measurement is firstly done on UV-VIS-NIR spectral range at λ = 300nm to λ = 2600nm. Since the absorption bandwidth is primarily at λ>3μm, the UV-VIS-NIR data is mainly supplementary but useful to check the correctness of the result. TE and TM polarizations are used to excite the proposed structure. It can be seen from Fig. 6(a) that the TE absorption gradually decreases when λ is approaching 2.6μm. The FTIR result in Fig. 6(b) further demonstrates the decent polarization selectivity of this proposal, where the measured TE absorption is suppressed to <0.1 for λ = 4μm to λ = 10μm, and the measured TM absorption is

Optics EXPRESS

>0.9 from λ = 4μm to λ = 7.54μm. It can be seen that the simulated and measured responses have close match except that the measured TE absorption is slightly higher than the calculated ones at λ<4μm, and the measured TM absorption is slightly higher than the calculated ones at λ>6μm. The higher measured TM absorption at λ>6μm is due to the light trapping effect associated with the ultrathin metallic films. The roughness of the e-gun evaporated ultra-thin metal and dielectric films leads to random light scattering and thus near-field absorption enhancement [40]. The higher measured TE absorption is due to the top and sidewall roughness at the aluminum wire-grids that similarly enhances the residual absorption for TE incidence. For longer wavelengths at λ>4μm, this TE absorption enhancement effect becomes less important because the gradually increased Al extinction coefficients (k) with wavelength lead to very high reflection even at the rough surface. The measurement set-up is illustrated in Figs. 6(c) and 6(d). It is worth to note that the current Al wire-grid has P = 1μm, and thus for λ>1μm the non-specular diffraction orders are evanescent modes. This point is very clear for those familiar with the coupled-wave analysis [37,38]. Since the polarization-selective absorption bandwidth is from λ = 4μm to λ = 8μm, integration sphere is totally not necessary. For improved performance, if desired, Ag or Au can be used with some risk of silicon contamination during IC processing.

4. Conclusion

For the first time, we experimentally demonstrate the ultra-broadband polarization-selective (PS) MPA. Our proposed design encapsulates advantages of polarization selection of wire grid structure as well as the simple planar configuration of MPA structures. At ultrathin metal thickness, the physics of field penetration does not change significantly with wavelength and thus contributes to an ultra-broadband absorption. Furthermore, the polarization selection due to Maxwell's boundary condition at the metal/air interface of the metallic wire-grid can persist over a very broad spectral range. Therefore, the metallic wire grid can be perfectly integrated with the thin-metal planar MPA design and leads to polarization-selective broadband absorption. The simulation results using wave optics RCWA calculation shows the proposed configuration can indeed be employed to realize strong polarization-selectivity. The absorption for TE incidence is <0.05 while the absorption for TM incidence is as high as >0.98, over λ = 1.48μm to λ = 4.27μm for t_{SiO2} = 80nm, P = 400nm, t = 300nm, and FF = 0.25. Further increase in bandwidth is done by using t_{SiO2} = 500nm where the polarization-selective absorption band spans from λ = 1.98μm to λ = 11.74μm with TM absorption >0.95 and TE absorption <0.04. Further decrease in TE absorption can be easily done by using Ag or Au but with the risk of silicon contamination. The measured result using UV-VIS-NIR and FTIR is consistent with the calculation result, and thus it is proved that the metallic wire grid ultrathin metal MPA can be truly polarization-selective over a broad spectral range with practical feasibility. We believe the proposed polarization-selective ultra-broadband MPA is never realized experimentally in literature, and the usefulness of this proposal can lie in remote sensing, biomedical imaging, energy harvesting, optical metrology and instrumentation.

Funding

The work is supported by the Ministry of Science and Technology (MOST), Taiwan, under grant number MOST 104-2221-E-009 –115 -MY2.